ACS APPLIED ELECTRONIC MATERIALS

pubs.acs.org/acsaelm

Article

Adhesion Microscopy as a Nanoscale Probe for Oxidation and Charge Generation at Metal-Oxide Interfaces

Alok Ranjan,* Andrea Padovani, Behnood Dianat, Nagarajan Raghavan, Kin Leong Pey, and Sean J. O'Shea*

Cite This: *ACS Appl. Electron. Mater.* 2023, 5, 5176−5186

Read Online

ACCESS | Metrics & More | Article Recommendations | Supporting Information

ABSTRACT: We introduce a method combining adhesion and conductivity measurements using conduction atomic force microscopy (AFM) to infer the localized surface redox reactions and charge generation resulting from defects created during the electrical stressing of a thin oxide film. The method is demonstrated on a 3.3 nm thick SiO_2, which is stressed by applying voltage to the AFM tip until soft dielectric breakdown (SBD) occurs, with the localized current−voltage characteristics and the tip−surface adhesion forces measured before and after the SBD event. The results show that under SBD, the field-driven diffusion of oxygen ions to the AFM tip leads to greatly enhanced adhesion because the oxygen reaching the surface forms strong chemical bonds with the tip material via oxidation. The electrical stressing also generates charged oxygen vacancy defects, and these are observed as an enhanced adhesion arising from image charge forces. The data presented can be corroborated to the physics of dielectric breakdown in transistor gate materials and conductive filament formation in memristor devices and could be extended to other technologies involving diffusion and surface reactivity of oxygen, e.g., solid oxide fuel cells and catalytic supports.

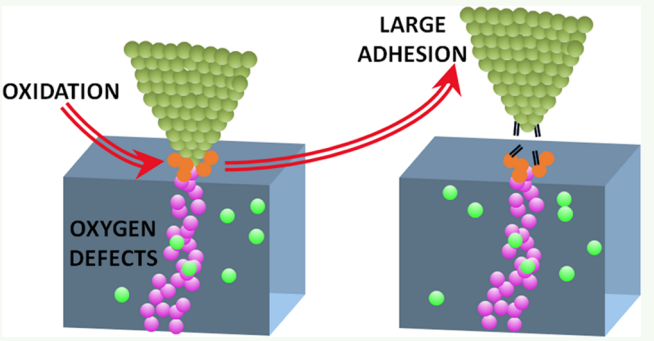

KEYWORDS: *oxygen defects, redox, image charge, adhesion, AFM and memristor*

INTRODUCTION

Electric field-driven diffusion and reactivity of oxygen in solid-state materials is fundamental to the working of several technologies based on solid oxides, such as resistive random access memory (ReRAM) elements,[1] electrical breakdown (BD) of the gate dielectric of field effect transistors (FET),[2] future thin-film ferroelectric memory and logic devices,[3] fuel cell anodes, and catalysis.[4,5]

The focus of the work presented here is on electronic applications. Device structures within electronic technologies are invariably driven toward miniaturization, and consequently, there is a need to understand oxygen diffusion and reactivity at a molecular level, not only to understand fundamental material transport phenomena that govern the device properties but also to improve the performance and/or reliability of the device and mitigate device failure. Here, we study the role of oxygen in the stress-induced electrical BD of the dielectric in FET logic devices, a key understanding required for ensuring reliability of the FET. Further, the results are directly relevant to oxygen-RAM devices (also called OxRAM or Valence Change Memory), a major class of ReRAM based on the formation of an oxygen vacancy filament linking the two device electrodes.[1] In OxRAM devices, oxygen ions are generated in the process of filament formation due to field- and charge fluence-induced metal−oxygen thermochemical bond breakage, and it is critical to understand both the reactivity of this oxygen with the electrode interfaces for device operation (switchability)[6] and if the oxygen reaches and escapes from the external electrode surface causing physical damage and device failure.[7] However, it is difficult to visualize or monitor oxygen and oxygen defects in solids on the nanoscale. Different measurement techniques for ReRAM applications, which can be generalized to other applications, can be applied,[8] and for nanoscale studies, the available approaches can be broadly summarized as methods based on either transmission electron microscopy (TEM) or scanning probe microscopy, with the latter being chiefly atomic force microscopy (AFM).

TEM provides a direct route toward understanding of oxide devices at the atomic scale, although the sample preparation can be difficult. Modern aberration-corrected TEM can provide sub-Angstrom spatial resolution, with chemical information simultaneously obtained using a suitable spectroscopic technique, e.g., lighter atoms such as oxygen can be

Received: July 5, 2023
Accepted: August 15, 2023
Published: August 29, 2023

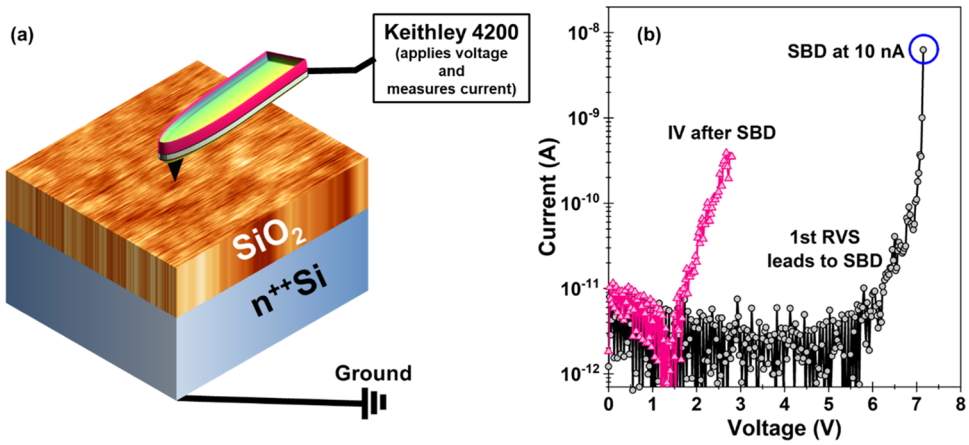

Figure 1. Current−voltage (I−V) measurements with CAFM on a thin oxide film. (a) The AFM operates in contact mode in UHV. Conducting diamond or all platinum wire tips are used. The voltage bias and current are applied/measured from the tip with a Keithley SCS 4200, an instrument that allows the current compliance to be limited to user-defined values as low as 0.1 nA, an important consideration to limit damage to the tip or sample from excessive current flow. (b) Two successive I−V curves taken on 3.3 nm thick SiO_2 with a 0.8 N/m Pt wire cantilever. The tip contacts the surface at user-defined location, and the current is measured as the voltage is linearly increased (a ramp voltage stress or RVS) until the current compliance is reached (10 nA in this example). Soft breakdown (SBD) occurs under this stressing condition as shown by the much lower resistance measured in the I−V taken immediately afterward.

detected with high sensitivity using electron energy loss spectroscopy (EELS).[9,10] While many in situ TEM studies have been undertaken to visualize and probe the diffusion and conducting path formation involving metal ions in ReRAM devices, there are fewer reports concerning oxygen in ReRAM because the atomic contrast is far weaker. Nevertheless, important insights have been obtained by high-resolution TEM (HRTEM) combined with EELS on the distribution and voltage-induced displacement of oxygen around an oxygen vacancy filament[11,12] and near the metal electrodes of HfO_2-[13] and strontium titanate[14]-based ReRAM. Advances in TEM methods and instrumentation will continue to impact the field. For example, a correlative study using atom probe tomography and TEM has recently been used to directly visualize oxygen (specifically ^{18}O isotope) residing at the grain boundaries of lanthanum chromite, a potential material for solid-state batteries and fuel cells,[15] and a novel electron beam-induced current (EBIC) imaging technique based on TEM was able to directly visualize changes in local conductivity arising from electrical stressing of a HfO_2 OxRAM structure.[16]

Of the AFM methods, Kelvin probe microscopy (KPM) and the related electrostatic force microscopy (EFM) measure the charge on a surface via changes in the electrostatic force acting on the AFM tip. These techniques have long been used to monitor changes in the accumulation or depletion of surface charge in oxides and other insulators under an applied voltage, including oxygen vacancy charge concentration.[17−19] A refinement of the electrostatic approach has recently been shown in which frequency modulation AFM (FM-AFM) was used on a strontium titanate crystal to monitor the migration of oxygen defects under the tip after the application of a voltage pulse.[20] In KPM and EFM, relative changes in charge distribution can be readily observed, but uncertainties in the modeling of the tip−sample electrostatic interactions, e.g., the influence of surface contaminants and unknown tip−sample geometry, make quantitative assessment of the charge density difficult.[21]

FM-AFM can also be used to image single oxygen atoms on surfaces prepared under ultrahigh vacuum (UHV) conditions,[22] with catalytic surfaces in particular being extensively investigated.[23] However, atomic-resolution AFM has not been extensively utilized in either oxide device or fuel cell studies because many of the materials of interest are amorphous, making high-resolution AFM imaging difficult.[24] One high-resolution AFM technique that is used extensively on thin-film oxides is conduction AFM (CAFM), in which a conducting tip is placed in contact with the surface.[25] By imaging the surface and simultaneously measuring the current flow at the tip, leakage current maps of the underlying material can be obtained with nanometer spatial resolution. Further, current−voltage (I−V) curves can be measured over defined locations of the surface, enabling individual resistive switching paths to be both formed and characterized at the nanoscale.[26] Charge trapping at single defects in the oxide may be observed as random telegraph noise in the current signal, indicating the location and to some extent energy levels of the defect.[27] An important new variation of CAFM for transport studies in oxides is electrochemical strain microscopy (ESM).[28] Here, a voltage bias is applied to the tip, which results in small changes in lattice strain due to the motion and/or generation of oxygen at the tip location, allowing mapping of the oxygen reactivity across the surface to be obtained. The correlation of the ESM signal with oxygen vacancy motion and localized I−V curves was shown for NiO crystals.[29] It is important to note that both the CAFM and ESM approaches use an electrode−oxide−electrode (i.e., tip−oxide−substrate) configuration and hence mimic realistic solid-state oxide devices.

In this work, we introduce another technique based on measuring adhesion by AFM. Adhesion AFM has yielded important insights ranging from the energy landscape of polymers, DNA strands, and proteins as they are unfolded by stretching,[30] to the role of adhesion in the wetting and friction properties of surfaces.[31] As in ESM, adhesion measurement is a mechanics-based approach and an indirect measure of oxygen charge or reactivity; hence, changes within the oxide material can only be inferred from the adhesion signal. Nevertheless, given that adhesion AFM is very well established, the research directions presented here can be developed as a generic approach to add to the understanding of solid-state oxide devices and materials.

https://doi.org/10.1021/acsaelm.3c00903
ACS Appl. Electron. Mater. 2023, 5, 5176−5186

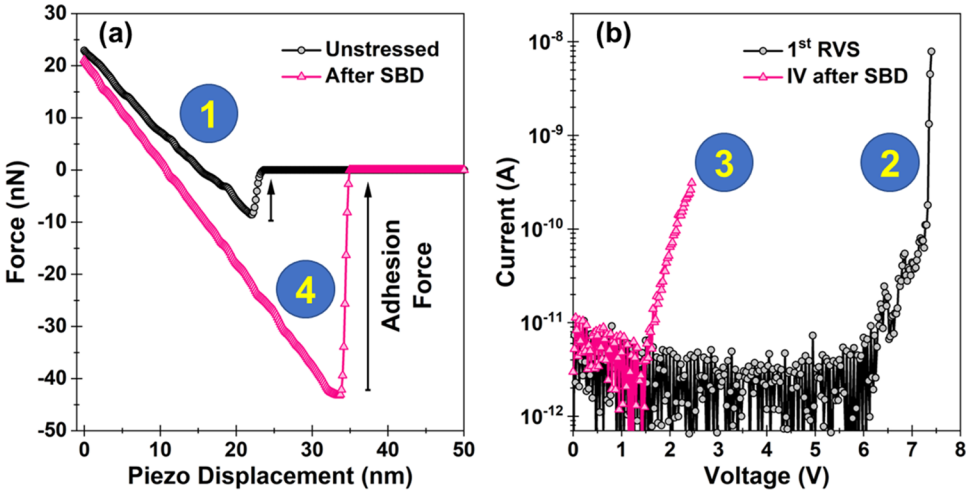

Figure 2. Experimental protocol to measure adhesion before and after electrical stressing by combining (a) force curves measuring adhesion and (b) $I-V$ curves measuring the charge injection and breakdown. The procedure, shown numbered, is as follows: (1) Measure the adhesion at a fresh surface location. (2) Stress the oxide (RVS) up to the chosen current compliance, e.g., 10 nA in this case. (3) Measure the $I-V$ at a lower voltage to check if the material has changed, e.g., undergone SBD. (4) Measure the adhesion after SBD. In the force curves, a more positive piezo displacement indicates the tip being pulled off the surface, and the adhesion force is given by the abrupt jump in the force as the tip detaches, e.g., at ~35 nm piezo displacement in the after-SBD curve.

In our approach, the adhesion measurements are combined with the CAFM method. CAFM is highly suitable for studying dielectric breakdown and ReRAM materials as both $I-V$ measurements and controlled breakdown/filament formation in the oxide can be undertaken by simply ramping the voltage applied to the tip, also called ramp voltage stressing (RVS). We demonstrate the method in a study of the dielectric breakdown of the thin-film SiO_2. The results show that the field-driven drift of oxygen to the top electrode (i.e., the AFM tip) leads to greatly enhanced adhesion because the oxygen reaching the surface chemically bonds with the tip material. This observation of oxygen reactivity at the metal electrode driven by the applied electric field is our key finding and supports both experimental and theoretical data showing oxygen diffuses to the oxide interface in gate dielectric breakdown.[32] Electrostatic image charge effects arising from the generation of charged oxygen vacancy defects are also observed at the breakdown location.

It is important to highlight that although we focus on dielectric breakdown, the results presented here are also equally relevant to any oxygen-based ReRAM, e.g., HfO_2 and Al_2O_3, where redox reactions[1,6] and oxygen gas evolution[7] at the metal-oxide interfaces play a critical role in the filament formation/rupture and device failure, respectively. Interestingly, SiO_2 itself is actively being investigated as a material for OxRAM as well.[7,33,34]

RESULTS AND DISCUSSION

Experimental Procedure. Experiments are undertaken with a deflection-type AFM in UHV operating at room temperature. Two types of conducting tips are used, namely, all-wire Pt tips and Si cantilevers coated with a conducting diamond film. The main sample investigated consists of a thermally grown 3.3 nm thick SiO_2 film on n^{++} ($\rho < 0.025$ Ω·cm) silicon substrate. For comparative purposes, data for a multilayer hexagonal boron nitride (h-BN) film on a polycrystalline copper substrate is also presented. Further experimental details are provided in the Experimental Section.

The CAFM setup is shown schematically in Figure 1a. For electrical measurements, the Si substrate is grounded, and a semiconductor characterization system measures $I-V$ data at the chosen locations on the surface (Figure 1b). Concurrently, force curves are used to measure the tip−surface adhesion force, as shown in Figure 2a. The adhesion force (F_{ads}) is given by the sharp jump in deflection as the tip pulls off the surface during the retraction part of the force curve. In our new experimental procedure, we combine the force curve (Figure 2a) and $I-V$ (Figure 2b) data acquisition. As shown in Figure 2, the adhesion is measured first at a new location to establish the adhesion reference value (Step 1). The voltage is then ramped (i.e., RVS) until the chosen current compliance is reached (Step 2), followed by an $I-V$ acquisition up to a smaller voltage to determine the change in conductivity due to dielectric breakdown (Step 3). Finally, the adhesion force is measured again after the electrical stressing (Step 4). Note that the tip remains at the same location for the entire procedure, which typically takes less than ~30 s to complete.

In Step 2, the voltage is ramped until the dielectric breakdown of the SiO_2 occurs, typically with the current compliance set at ~10 nA. The breakdown of SiO_2 has been extensively studied both for semiconductor FET reliability[2,35,36] and potential ReRAM application.[33] Thin SiO_2 films show gradual electrical degradation under increasing electrical stress. There is an initial stage characterized by a slow increase in the leakage current arising from the creation of defects in the SiO_2 lattice. Various possible defects[37] can form, but in the breakdown of amorphous SiO_2, the neutral oxygen vacancy (V_O) has been identified as the most probable species responsible for the trap-assisted tunneling of charge carriers[33,36,38] between the electrodes. Interstitial oxygen ions (O^{2-}) are created during the formation of the Vo traps. As electrical stressing continues, a sufficient number of V_O defects in close spatial proximity are generated such that a high-conductivity path (called a percolation path) forms across the electrodes, and the current flow abruptly increases by several orders of magnitude (see Figure 1b). We define this abrupt current increase as dielectric breakdown. Further stressing

https://doi.org/10.1021/acsaelm.3c00903
ACS Appl. Electron. Mater. 2023, 5, 5176−5186

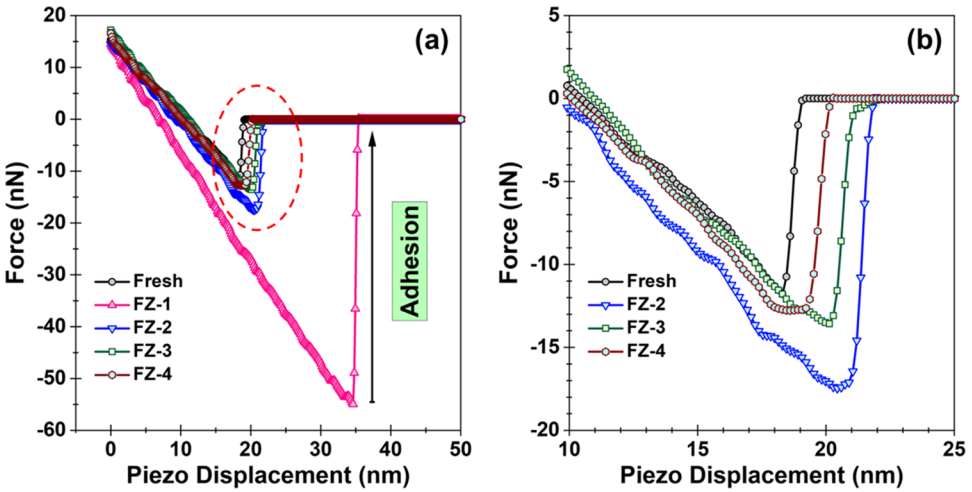

Figure 3. Successive force curves taken at a location subjected to SBD. (a) The adhesion measured on the fresh surface is −11.5 nN. RVS is then performed such that the SiO_2 undergoes SBD using a current compliance of 10 nA at positive tip bias, after which the first force curve (FZ-1) shows a considerably larger adhesion (−55 nN). The subsequent measurements (FZ-2 to FZ-4) show that the adhesion remains slightly higher than the fresh surface and decreases over time due to either thermal drift of the tip away from the BD location or a decrease in charge with time at the BD location. Note that a more positive piezo displacement indicates the tip being pulled off the surface. (b) Expanded view of the circled region in (a). A diamond cantilever (1.6 N/m and R_{tip}= 120 nm) is used.

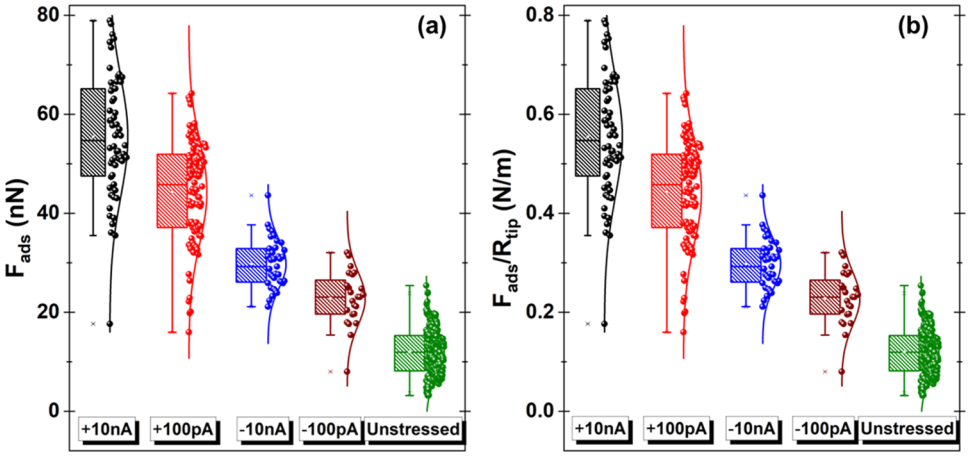

Figure 4. Summary of data measuring the adhesion of the first force curve taken after SBD of the SiO_2. Each dot represents a separate experiment following the procedure of Figure 2. (a) Data taken using two different tips at positive or negative tip bias and using 100 pA or 10 nA current compliance for the RVS stressing. There is statistical scatter in any adhesion measurement, but the results clearly show the adhesion is enhanced after RVS stressing and the effect is far more pronounced at positive tip polarity. (b) Data of (a) normalized to the tip radius (R_{tip}), which allows comparison between different tips since F_{ads}/R_{tip} approximately equates to the adhesion energy. The two tips used are diamond cantilevers (1.6 N/m and R_{tip}= 120 nm;1.3 N/m and R_{tip} = 100 nm).

leads to rapid growth of the breakdown spot and broadly; there are two routes of the spot evolution.[35] For thick films and/or high voltages, a catastrophic failure of the SiO_2 occurs, termed hard breakdown, involving high-current-density-induced thermomigration of Si substrate material, large power dissipation, thermal stresses, and material damage at the breakdown location. For thin films (<∼3 nm thickness) and/or low voltages, a much slower increase in conductivity is observed with no physical change in the morphology of the BD region in SiO_2, which is termed as progressive or soft breakdown (SBD). This mechanism also forms the basis of OxRAM device operation.[8,33] SBD is the breakdown condition exclusively observed in the work presented here.

Adhesion Results on Electrically Stressed SiO_2. Figure 3 shows force curves taken after electrical stressing and highlights the main result found. Specifically, we observe that the first force curve taken after RVS stressing *at* positive tip polarity (curve FZ-1 in Figure 3a) shows significantly enhanced adhesion compared with the pristine SiO_2 surface. The next force curves taken immediately afterward at the same location show much lower adhesion (Figure 3b), but the adhesion is always higher than the value of the unstressed film. Data taken at negative tip polarity also show higher adhesion compared to the unstressed film, but with the important difference that the first force curve after stressing is not significantly enhanced (see Figure S1).

Adhesion measurements are statistically variable, and many data sets need to be collected to undertake analysis or evaluate trends. Figure 4 presents an example of our experiments and shows the variation in the adhesion of the first force curve after electrical stress at different current compliances. Each point represents one adhesion measurement, following the protocol

https://doi.org/10.1021/acsaelm.3c00903
ACS Appl. Electron. Mater. 2023, 5, 5176−5186

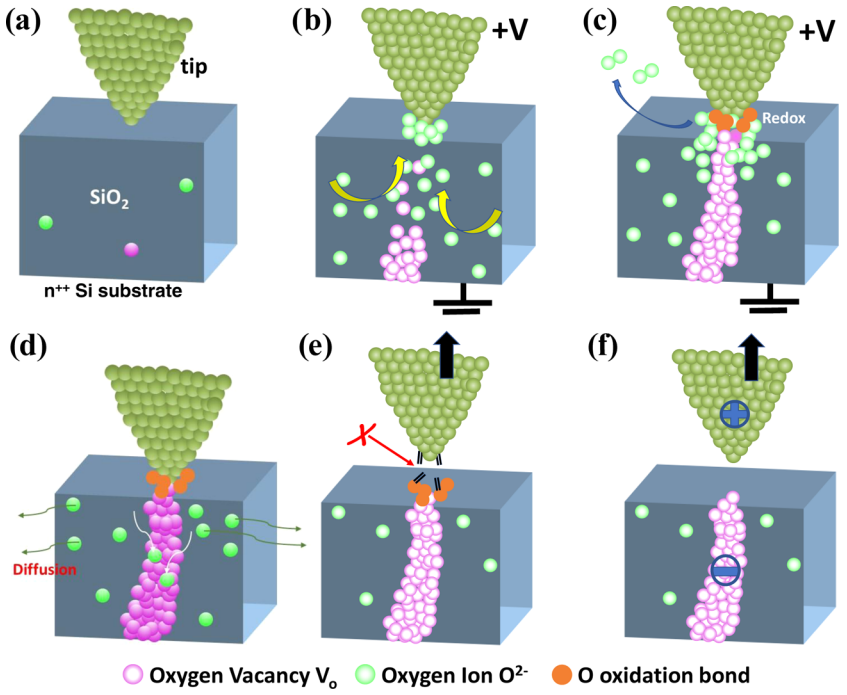

Figure 5. Schematic of the underlying adhesion mechanisms on electrical stressing of SiO_2. (a) The pristine SiO_2 film has few defects. (b) On stressing the Si−O−Si bond structure is disrupted, generating (principally) neutral oxygen vacancy defects (V_O) and O^{2-} ions. (c) As stressing continues and defect generation intensifies, the V_o defects form a conducting percolation path between the electrodes resulting in soft breakdown. If the tip bias is positive (+V), the O^{2-} ions move to the tip-SiO_2 interface enabling redox reaction (ionic or covalent bond formation) with the tip material. (d) When stressing stops and the bias is removed, the O^{2-} ions diffuse away from the breakdown location, whereas the V_o defects are relatively immobile. (e) The first adhesion curve after SBD breaks the chemical bonds formed at the surface and the adhesion is high. (f) Subsequent force curves still show enhanced adhesion compared with pristine SiO_2 because of an image charge force arising from the fixed charge of the immobile V_o, which are predominantly negatively charged as the V_o defects are deep electron traps.

of Figure 2. We observe that the adhesion always increases after stressing compared to the fresh surface. The change in adhesion after stressing at positive bias (using +100 pA or +10 nA compliance) is approx. 2−3 times as large as at negative bias (using −100 pA or −10 nA compliance). This strong difference in adhesion with stressing polarity is always observed (see also Figure S1). There is a slight increase in adhesion as the current compliance increases from 100 pA to 10 nA, but this effect is relatively small and not always clearly observed (see Figure S2).

Figure 4b replots the data of Figure 4a as F_{ads}/R_{tip}, where R_{tip} is the estimated radius of the tip apex as measured by scanning electron microscopy (Figure S3). The quantity F_{ads}/R_{tip} approximately equates to the adhesion energy as $F/R_{tip}= 2\pi W_{flat}$, where W_{flat} is the adhesion energy per unit area of two flat surfaces[39] in contact. Normalizing the adhesion force in this way therefore allows data obtained on different surfaces or tips to be compared, although even with this procedure the statistical nature of adhesion measurement leads to a large scatter of the data, e.g., the adhesion energy for the first force curve after stressing varies between ∼40 and 100 mJ/m^2 for different tips. Note that the F/R_{tip} normalization is useful for comparing different tips on identical surfaces, e.g., either the SiO_2 surface before SBD or after SBD. However, in our experiments, the change in surface energy itself arising from the SBD cannot be found with this simple approach because, as detailed in Note S1, the effective area over which electrical breakdown occurs under the tip is far smaller than the geometric tip−surface contact area (approx. 10−100 nm^2). Changes in surface heterogeneity must be modeled using more advanced approaches such as the surface element integration method[40,41] to separate the contributions of the force arising from just the surface area influenced by the SBD and the rest of the tip.

We observe similar trends to Figures 3 and 4 with both Pt and diamond tips (Figure S4). Experiments were also undertaken with the sample held at 250 °C and a base pressure of <2 × 10^{-9} Torr (Figure S5). The adhesion decreases at high temperatures as expected because adhesion is a thermally activated process, but the trend of increased adhesion after electrical stressing, including the enhanced adhesion in the first force curve after RVS stressing at positive polarity, is clearly observed even at 250 °C. This result indicates that adsorbed water, which can reside on surfaces even under UHV, does not influence the data. This is important as it is well known that anodic oxidation and similar electrochemical effects can take place under high electric field[42] using CAFM, potentially giving rise to an increase in mechanical adhesion from the buildup of material around the tip.

Physical Basis for Enhanced Adhesion after Electrical Stressing. Figure 5 summarizes the most plausible explanation of the experimental data detailed above and follows from the present understanding of breakdown and filamentary switching mechanisms in ReRAM for thin-film oxides.[1,2,32,36] There are few electronic defects in pristine SiO_2 film,[43] and the measured adhesion (Figure 5a) arises from the mechanical and van der Waals interactions of the tip−surface contact.[39] When a strong electric field is applied across the film, Si−O−Si bonds can break and generate defects in the film (Figure 5b), which

https://doi.org/10.1021/acsaelm.3c00903
ACS Appl. Electron. Mater. 2023, 5, 5176−5186

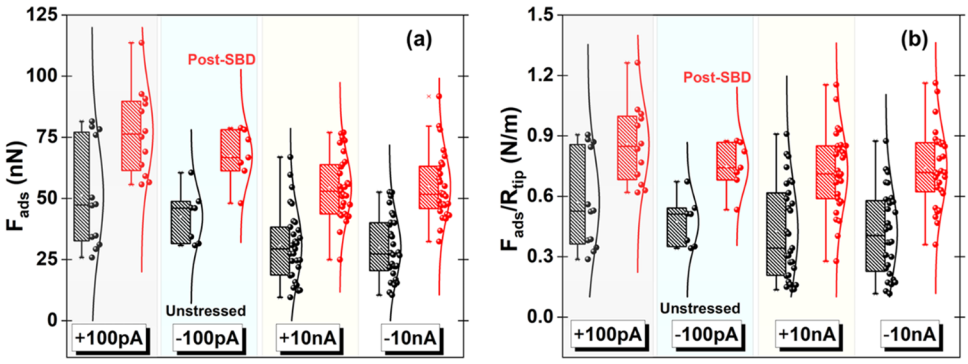

Figure 6. Few-layer h-BN film mainly shows an image charge force after RVS stressing. (a) Data comparing the adhesion on a pristine surface (labeled Unstressed) with adhesion of the first force curve taken after RVS stressing (labeled Post-SBD). The data is taken using two different tips at positive or negative tip bias and using 100 pA or 10 nA current compliance for the RVS stressing. There is a small increase in adhesion after stressing, presumably from image forces created by the charge injection into the film, but the absence of any large increase in adhesion or polarity dependence suggests no significant chemical bond formation occurs at the h-BN/tip interface. (b) Data of (a) normalized to the tip radius (R_{tip}). The two tips used are diamond cantilevers (0.33 N/m and R_{tip}= 100 nm; 0.28 N/m and R_{tip} = 120 nm).

in amorphous SiO_2 are primarily the neutral V_O defect and the O^{2-} ions. As electrical stressing continues, the O^{2-} ions will migrate toward the positively biased electrode, and oxidation, i.e., redox reactions, can cause the formation of chemical bonds between the electrode (tip) and SiO_2 (Figure 5c). An atomistic understanding of the tip-SiO_2 bond formation is lacking at present, but corroborative studies are discussed below. In particular, it has been shown that molecular oxygen (O_2) is produced at the breakdown location,[32] as indicated in Figure 5c by O_2 exiting the film, from which it was concluded that the generated O^{2-} migrate to the electrode where they discharge and recombine into O_2. Similarly, in OxRAM devices, deformation and blistering of the electrode have been observed in filament formation as O_2 is ejected from the oxide forming cavities at the electrode−oxide interface.[44,45]

Once the electric field is removed (Figure 5d), the O^{2-} diffuse rapidly away as the barrier[38] for O^{2-} migration is only ∼0.2 eV. In contrast, the diffusivity of V_O is far less, with the barrier for V_O migration being 3.2 to 5.6 eV,[33] i.e., the chain of V_O defects linking the tip and Si electrode is essentially static. The chemical bonds created by oxidation at the tip-SiO_2 interface lead to the high adhesion observed when the tip is initially pulled off the surface (Figure 5e). The lower adhesion found in subsequent measurements occurs because no chemical bonds are present (Figure 5f); the bonds were already broken in the first adhesion measurement. There is still an increase in adhesion compared to pristine SiO_2 because electrostatic interaction occurs; i.e., there is an image charge force between the tip and fixed charge in the film. The mobile O^{2-} ions diffuse away from the stress location and do not contribute to the image charge force. The fixed charge is most likely the negatively charged oxygen vacancy (V_O^-) because it has been shown that the neutral V_O generated in amorphous SiO_2 can transform to negative V_O^- by trapping[37,38] one or two electrons. Since the V_O electron traps are very deep,[37] the negative V_O^- state is stable.[36]

At negative polarity, defects are also generated in the SiO_2 film during electrical stressing, leading to an increase in adhesion because of image charge forces from the fixed V_O^- charge created at the breakdown location. However, a large adhesion is not found in the first adhesion measurement after RVS stressing because chemical bonds do not form between the tip and surface as at negative polarity, the O^{2-} ions drift toward the bottom electrode (Si substrate). Hence, oxidation at the tip−surface interface does not occur.

Identical experiments undertaken on a few-layer h-BN film (2−5 nm thick) support the above interpretation as well. As shown in Figure 6, we do not observe a large adhesion in the first force curve after RVS stressing with either positive or negative bias polarity. Only a small increase in adhesion is observed after electrical stressing, consistent with an image charge force arising from the generation of trapped charge in the h-BN, most likely boron vacancies.[2] There is no chemical bond formed at the AFM tip/h-BN interface because no chemical species are generated that can react with the tip electrode. It is also known that h-BN acts as a diffusion barrier,[46] which would hinder out-of-plane migration of any reactive species toward the tip region.

The strong adhesion in the first force curve after RVS stressing also leads to appreciable effects on friction (Figure S6). This observation provides additional evidence of chemical bonding because friction forces are highly sensitive to the chemical interactions[39] occurring between sliding surfaces. We rule out any significant physical (geometric) effects from changes in the tip−sample contact after stressing. AFM imaging of the identical SiO_2 surface shows small hillocks or protrusions may occur at the breakdown location after SBD.[47] However, the hillocks are always very shallow, being ∼1 nm in height over 10 nm or more length[48] and the tip will see the surface as essentially being flat as far as adhesion is concerned. Further, the second, third, and fourth adhesion measurements are taken at the same location as the first adhesion measurement but do not show a similar large adhesion that would presumably occur if geometric changes from hillock formation were causing enhanced adhesion.

The evidence for V_O and O^{2-} defect creation and diffusion in oxide films under electrical stress is well established. The question arises as to how this changes the adhesion measured at the electrode−oxide interface. This is a complex issue that cannot be fully answered at present as oxide surfaces interact in myriad ways with other materials.[49] Broadly, we separate the adhesion as arising from either chemical bonding at the tip−sample interface or image charge forces due to the presence of ions at or near the tip−sample interface. We ignore van der Waals and electrostatic forces, which contribute to adhesion on

https://doi.org/10.1021/acsaelm.3c00903
ACS Appl. Electron. Mater. 2023, 5, 5176−5186

the pristine surface as the objective is to understand the difference in adhesion before and after electrical stressing.

Chemical Bonding-Enhanced Adhesion of the First Force Curve at Positive Bias. Adhesion is correlated to the formation of bonds at the interface,[50] and in oxides, strong polar or covalent bond formation often arises from charge transfer and the resultant chemical reactions at the metal-oxide interface. Fu and Wagner[49] identify four general reaction mechanisms at metal-oxide interfaces, namely, redox reactions, alloy formation, encapsulation of nanoparticles (NP), and interdiffusion of metal, all of which have been observed in the SiO_2-metal systems. A redox mechanism, i.e., oxidation of the electrode material, appears to be the most likely explanation of our results as it is the only mechanism involving oxygen mass transfer at room temperature (RT). The alternative mechanisms of encapsulation (i.e., the mass transport of oxide to cover or immerse adsorbed NP) or the diffusion of metal into the SiO_2 to form interfacial alloys or silicides require annealing at high temperatures (typically >∼600 °C).[51] High temperatures are not expected in our experiments because the low current used (0.1−10 nA) ensures Joule heating is small.[2] High electric fields can also drive the diffusion of metal into oxide, and given that the applied field in our experiments is as high as ∼20 MV/cm, a possible path leading to increased adhesion is the formation of a silicide at the Pt−SiO_2 interface by field-driven diffusion from the Pt tip into the SiO_2 at positive bias. We consider this unlikely because Pt does not react with SiO_2 at RT[51] or form alloys,[52] even when heated at 800 °C vacuum.[53] Further, HRTEM studies of ReRAM filament formation show that although field-induced migration of noble metals can occur in evaporated or sputtered SiO_x film,[54,55] no migration can be observed in high-quality oxides,[55] as used here. We note that more reactive metals (e.g., Zr, Ti) could behave quite differently with regard to silicide formation.

Our assertion is that the markedly increased adhesion on the first pull-off curve is due to a redox reaction between the AFM tip and the O^{2-} ions that have reached the SiO_2−tip interface. This is supported by indirect observations in the filament formation of OxRAM devices in which once SBD occurs, the oxygen ions react with anode materials,[1] and in particular with reactive metal electrodes, thereby oxidizing them partially. As also noted by Shluger and co-workers,[32] the release of O_2 from electrically stressed SiO_x implies an interaction of oxygen ions with the top electrode material.

However, the specific atomic bonding involved is unknown. It has been demonstrated that redox reactions require oxygen ions to diffuse to the interface from the bulk oxide,[49] as also occurs in our experiments, but experimentally the systems previously studied involve reactive electrodes and oxides, e.g., $SrTiO_2$ and TiO_2. Similarly, computational studies typically investigate reactive systems, and few explicitly consider adhesive bonding with SiO_2. An example is the DFT study of Tea et al.[56] who investigated atomic bonding and adhesion of Al to SiO_2 with and without V_O at the interface since Vo defects are very common at silica surfaces.[49] They find that the adhesion is smaller in the presence of V_O surface defects because the missing oxygen in the SiO_2 lattice removes the Al−O bonds associated with that oxygen, leaving 2 × Si−Al bonds at the interface compared with 1 × Si−Al/2 × O−Al bonds of the defect-free SiO_2. Our experiments are notably different as our Pt and diamond electrodes are far less reactive (electronegativity χ = 2.5) than Al (χ = 1.5), the adhesion increases as V_O defects are generated, and bonding to V_O defects cannot explain why enhanced adhesion only occurs at positive polarity. We have discussed this study[56] in detail because it highlights the necessity of investigating the specific interface of interest to extract meaningful data. Unfortunately, no similar computational study exists to elucidate the bonding of our electrode materials (Pt, diamond) to SiO_2 in the presence of excess O^{2-} or V_O defects. Nevertheless, a related question that can be answered is that previous work has shown that redox reactions with the O^{2-} ions are certainly feasible in the oxidation of both Pt and diamond, as now discussed.

Oxidation of the Tip Material. The oxidation behavior of many surfaces has been extensively investigated using techniques such as HRTEM, EELS, Auger electron spectroscopy, X-ray photoelectron spectroscopy, scanning tunneling microscopy, etc. It is found that both tip materials, Pt and boron-doped diamond (BDD), in general, do not easily oxidize and require high temperatures for reaction with molecular oxygen. However, both readily react with atomic oxygen at room temperature.

Oxidation of Pt has been extensively studied in the gas phase because of the critical utility of Pt as a catalyst in the reduction of organic compounds, fuel cell anodes, and automotive exhaust treatments.[4] Molecular oxygen needs to dissociate to form an oxide on a Pt surface, and although this can occur at RT, the oxygen coverage is low, around 0.25 monolayer on crystalline Pt surfaces.[57] Thus, oxidation of Pt is difficult at RT[4] and temperatures >800 °C are typically required to fully oxidize crystalline Pt in O_2.[58] Platinum NP behaves somewhat differently in that very small NP (<6 nm diameter) will oxidize when exposed to ambient O_2, but only the very smallest NP (<1.5 nm diameter) completely oxidize.[59,60] Importantly for our work, the situation is very different when Pt is exposed directly to atomic oxygen as in this case, the surface of Pt NP readily oxidize at RT, typically forming PtO or PtO_2 species.[4,61]

Diamond (BDD) finds application as an extremely robust electrode material in sensors and biomedical technology, and hence, the relevant literature is largely directed toward electrochemical studies. BDD can be oxidized electrochemically, thermally (e.g. heating to ∼600 °C in air), and by ozone and oxygen plasma exposure to generate hydroxyl (C−OH), ether (C−O−C), and carboxyl (C═O) surface groups.[62,63] Only a few research groups have investigated polycrystalline or crystalline diamond under vacuum conditions.[64−66] Polycrystalline BDD is typically grown by chemical vapor deposition and produces a hydrogen-terminated surface (h-BDD). These studies reveal that molecular oxygen has little interaction with the diamond surface[64] and h-BDD is essentially inert at temperatures below ∼900 °C.[65] In contrast, exposure to atomic oxygen readily oxidizes h-BDD[64] and the crystalline (100)[65] and (111)[66] surfaces at RT, with the oxygen bonding to the surface as carbonyl, ether, or peroxide (C−O−O-C) groups.

From these previous studies, we can conclude that BDD and Pt can oxidize in the presence of atomic oxygen at RT and that the flux of O^{2-} ions generated under stressing can increase adhesion by creating bonds via redox reaction at the Pt/diamond-SiO_2 interface. The oxidation process at the interface is not known, other than the inference that increased adhesion strongly implies covalent or polar bonding between the surface Si−O and the Pt or diamond tip.

https://doi.org/10.1021/acsaelm.3c00903
ACS Appl. Electron. Mater. 2023, 5, 5176−5186

Adhesion from Tip-SiO_2 Image Charge Force. When two surfaces come into contact, charge redistribution occurs at the interface, giving rise to electrostatic interactions between the two contacting materials. Such interactions can contribute a significant or dominant part of the adhesion energy between metal-oxide surfaces, as first described by Stoneham and co-workers.[67,68] Charged defects in the oxide typically increase the adhesion energy because the image charge force acting between the defects and the metal layer is attractive. Here, we are concerned with the change in adhesion after SBD rather than the fundamental adhesion of the initial surface contact, with the observed increase in adhesion after SBD (excluding the first adhesion measurement at positive bias) being the result of the generation of fixed oxygen vacancy charge (negative V_O^-) at the SBD location inducing an image charge force on the AFM tip. Image charge forces have been known for some time to enhance adhesion at metal-oxide interfaces,[50,68,69] and our results provide further evidence for this phenomenon at the nanoscale. Our assertion that charged V_O defects are the major contribution to the observed image force is supported by many previous studies which highlight that introducing charged V_O defects in an oxide can greatly increase the metal-oxide interfacial adhesion, e.g., in MgO,[70,71] ZrO_2,[50] and TiO_2.[71]

We expand on this viewpoint by estimating the number of charged defects (N_Q) that give rise to the measured adhesion after electrical stressing. Details are provided in Note S1. The generation of N_Q charged defects localized at the breakdown spot gives rise to an image force (F_{img}) of,[72]

$$F_{img} \approx -\frac{N_Q^2 q^2}{16\pi\varepsilon_0}\frac{1}{S^2}\left(\frac{\varepsilon_0 - 1}{\varepsilon_{0x} + 1}\right) \quad (1)$$

where q is the electron charge, s is the distance of the net effective charge ($q \times N_Q$) from the tip-SiO_2 interface, ε_0 is the vacuum permittivity, and ε_{ox} is the oxide relative permittivity. Experimentally, F_{img} is the enhanced adhesion measured after RVS excluding the first adhesion curve taken at positive polarity. The value is found from the difference in adhesion between the pristine substrate and either (i) the adhesion after RVS at negative polarity or (ii) the adhesion measured in the second or subsequent force curve after RVS at positive polarity. Taking data of Figure 3b as an example, F_{img} = 6 nN after SBD, from which we find N_Q = 21, i.e., 21 charges, presumably V_O^-, have been created in the SiO_2 at the breakdown location under the tip. Converting this value to a volume charge density (N_Q^V) yields values of $N_Q^V \approx 0.5$ to 6×10^{20} cm^{-3}, depending on the chosen size of the SBD spot. These values compare favorably with values of the critical defect density required for oxide BD in percolation models[73] and the trap defect density supporting the SBD current estimated by detailed charge transport simulations.[74] Although several approximations have been made in these estimations, the outcome is reasonable and the approach outlined in Note S1 could be further refined to provide a quantitative methodology for the measurement of trapped charge at the nanoscale.

CONCLUSIONS

The approach presented here shows that measurement of adhesion by AFM provides additional information about localized oxidation and charge generation induced by electrical stressing of thin-film dielectrics. The electrical stressing is undertaken using conduction AFM, which also allows nanoscale $I-V$ data to be collected. This combination of adhesion and CAFM measurements is particularly insightful in furthering our understanding of the breakdown of thin-film gate dielectrics and the related topic of oxygen vacancy filament formation in OxRAM devices. As an example, we described in detail here our studies of the SBD of SiO_2 where we find the generation of oxygen ion and oxygen vacancy defects by SBD leads to increased adhesion via (i) redox reactions of the oxygen ions with the tip material, leading to the formation of chemical bonds at the SiO_2/tip interface, and (ii) image charge forces arising from charged oxygen vacancies created at the SBD location. We believe the approach here can be further developed given the maturity of adhesion force microscopy and extended to catalytic surfaces and tip materials in which oxidation and chemical bond formation is important.

EXPERIMENTAL SECTION

UHV System. Experiments are undertaken with a deflection-type AFM in UHV (RHK Technology) operating at room temperature with a base pressure of 2×10^{-10} Torr. Argon ion milling (Vacuum Microengineering IPS3-D fitted with ion gun IG70) is used for cleaning residues and contaminants from the AFM tip, with typical ion milling conditions of Ar pressure of 5×10^{-6} Torr, acceleration voltage of 1.2 kV, and ion current of 8 μA measured at the tip. Samples can be heated in situ by a filament placed directly under the sample with the temperature measured by a thermocouple clamped onto the sample surface.

Samples and Tips. High-quality SiO_2 film is thermally grown on n^{++}Si ($\rho < 0.025$ Ω·cm) substrate. The n^{++}Si substrate is precleaned in HF solution to remove native oxide prior to the thermal growth of SiO_2. The SiO_2 thickness measured using an ellipsometer and cross-sectional TEM measurements is 3.3 nm. The multilayer h-BN film is supplied by Graphene Supermarket and is grown on a polycrystalline copper substrate. The grain size of the Cu as measured by AFM is between 10 and 100 μm, and cross-sectional TEM shows that the thickness of the h-BN film varies between 2 and 5 nm. All of the SiO_2 and h-BN samples were mildly heated (~80 °C) at least once under UHV prior to use to help remove adsorbed water.

Two types of conducting tips are used: all-wire Pt tips from Rocky Mountain Nanotechnology (12Pt300 nominally 0.8 and 25Pt300 nominally 18 N/m) and rectangular Si cantilevers coated with a conducting diamond film from NanoWorld AG, Switzerland (CDT-FMR nominally 1.2−5.5 N/m and CDT-NCLR nominally 31−71 N/m). The tips are always ion-milled for ~4 min when first inserted into the UHV chamber. During experimentation, the tips may become poorly conducting, even under UHV conditions, and in these cases, the tip can be ion-milled to try to revert back to the original tip conductivity. All tips are imaged after the experiments in a SEM to provide an indication of both R_{tip} and the integrity of the diamond film coating on the tip apex.

CAFM Electrical Measurements. The n^{++}Si substrate is electrically grounded, and the cantilever is connected to a Keithley semiconductor characterization system (SCS 4200). The SCS 4200 both applies voltage bias and measures the current from the tip to measure $I-V$ curves. The compliance current can be limited to defined values by the SCS 4200, ensuring high current flow and transient current overshoot at BD do not occur, both of which can damage the tip or the sample. This is important as in the experiments, the voltage is ramped until SBD of the SiO_2 occurs, typically with a current compliance ~10 nA, and if the current were not limited, hard breakdown would occur with associated Joule heating and catastrophic physical changes (material removal) of the sample or tip.

AFM Force Measurements. Force curves are used to measure the tip−surface adhesion force. As the AFM experiments are undertaken in contact mode, i.e., the tip always remains in contact with the surface, the force curves are straightforward. The static deflection of the cantilever is recorded as the tip is moved toward and away from the surface. The static defection signal is approximately

https://doi.org/10.1021/acsaelm.3c00903
ACS Appl. Electron. Mater. 2023, 5, 5176−5186

linear for two hard surfaces in contact (see Figure 2a), and the force acting on the tip (F) is simply $F = k_c\Delta z$, where k_c is the cantilever spring constant and Δz is the displacement of the tip in the surface normal direction. The adhesion force (F_{ads}) is given by the sharp jump in deflection as the tip pulls off the surface during the retraction part of the force curve. Note that F_{ads} is by definition negative, but for clarity, this distinction is ignored in the discussions.

An accurate value of k_c is required to convert static cantilever deflection to a force. Calibration procedures to find k_c are well documented,[75] and here, we only note two relevant aspects. First, for diamond cantilevers, an accurate value of the lever thickness is found by measuring the resonance frequency of the cantilever, from which k_c can be calculated using the known material properties, width and length of the cantilever.[76] This approach is reasonable, as the diamond cantilevers have well-defined rectangular dimensions. However, the method cannot be used for all-wire Pt cantilevers, as the geometry of these levers is highly irregular. Hence, the manufacturer values of k_c are used for the Pt wire levers. Second, the slope of the force curve provides the calibration sensitivity, i.e., the conversion of the cantilever deflection signal (in Volts) to nanometers. We do not correct the slope calibration for the tilt of the cantilever[77] as this effect is small. However, we do note that the slope is steeper for the first force curve measured after the SiO_2 SBD (see curve FZ-1 in Figure 3a). In this case, the tip is effectively pinned at the tip apex by very strong adhesion of the SiO_2−tip chemical bonding. The pinning of the tip deforms the shape of the cantilever beam as it is retracted, and the shape deformation in turn influences the response of the laser spot reflected from the lever. An analytical correction for this effect is nontrivial as the precise location of the laser spot on the lever is required. However, comparing the slopes for low and high adhesion cases of ∼100 force curves shows that the steeper slope could underestimate the values of adhesion where such pinning occurs by ca. 20−25% at most.

■ ASSOCIATED CONTENT

Supporting Information

The Supporting Information is available free of charge at https://pubs.acs.org/doi/10.1021/acsaelm.3c00903.

Experimental data on SiO_2 and relation between the measured adhesion force and the image force arising from fixed charge in the SiO_2 film (SI Note S1) (PDF)

■ AUTHOR INFORMATION

Corresponding Authors

Alok Ranjan − *Division of Nano-and-Bio Physics, Department of Physics, Chalmers University of Technology, Gothenburg 41296, Sweden; Engineering Product Development, Singapore University of Technology and Design, 487372, Singapore;* orcid.org/0000-0003-4592-1674; Email: alok.ranjan@chalmers.se

Sean J. O'Shea − *Institute of Materials Research and Engineering, Agency for Science Technology and Research, 138634, Singapore;* orcid.org/0000-0003-0385-6245; Email: s-oshea@imre.a-star.edu.sg

Authors

Andrea Padovani − *Dipartimento di Ingegneria Enzo Ferrari, University of Modena and Reggio Emilia, Modena 41125, Italy*

Behnood Dianat − *Dipartimento di Scienze e Metodi dell'Ingegneria, University of Modena and Reggio Emilia, Modena 42122, Italy*

Nagarajan Raghavan − *Engineering Product Development, Singapore University of Technology and Design, 487372, Singapore;* orcid.org/0000-0001-6735-3108

Kin Leong Pey − *Engineering Product Development, Singapore University of Technology and Design, 487372, Singapore;* orcid.org/0000-0002-0066-091X

Complete contact information is available at: https://pubs.acs.org/10.1021/acsaelm.3c00903

Notes

The authors declare no competing financial interest.

■ ACKNOWLEDGMENTS

The authors greatly appreciate discussions with D. Srolovitz (Department of Mechanical Engineering, The University of Hong Kong) on the atomic level behavior of interfaces and A. Shluger (University College London) for initially suggesting that chemical bonding may be at play at the SiO_2 surface after breakdown. They also thank J. Molina (National Institute of Astrophysics, Optics and Electronics, Mexico) for providing SiO thin films used in this study. Alok Ranjan acknowledges Chalmers University of Technology for providing support for the open-access publications.

■ REFERENCES

(1) Zahoor, F.; Zulkifli, T. Z. A.; Khanday, F. A. Resistive random access memory (RRAM): An overview of materials, switching mechanism, performance, multilevel cell (mlc) storage, modeling, and applications. *Nanoscale Res. Lett.* **2020**, *15* (1), No. 90.

(2) Palumbo, F.; Wen, C.; Lombardo, S.; Pazos, S.; Aguirre, F.; Eizenberg, M.; Hui, F.; Lanza, M. A review on dielectric breakdown in thin dielectrics: Silicon dioxide, high-k, and layered dielectrics. *Adv. Funct. Mater.* **2020**, *30* (18), No. 1900657.

(3) Nukala, P.; Ahmadi, M.; Wei, Y.; de Graaf, S.; Stylianidis, E.; Chakrabortty, T.; Matzen, S.; Zandbergen, H. W.; Björling, A.; Mannix, D.; Carbone, D.; Kooi, B.; Noheda, B. Reversible oxygen migration and phase transitions in hafnia-based ferroelectric devices. *Science* **2021**, *372* (6542), 630−635.

(4) Ono, L. K.; Croy, J. R.; Heinrich, H.; Cuenya, B. R. Oxygen chemisorption, formation, and thermal stability of Pt oxides on Pt nanoparticles supported on SiO_2/Si(001): Size Effects. *J. Phys. Chem. C* **2011**, *115* (34), 16856−16866.

(5) Mahato, N.; Banerjee, A.; Gupta, A.; Omar, S.; Balani, K. Progress in material selection for solid oxide fuel cell technology: A review. *Prog. Mater. Sci.* **2015**, *72*, 141−337.

(6) Liu, K.; Qin, L.; Zhang, X.; Zhu, J.; Sun, X.; Yang, K.; Cai, Y.; Yang, Y.; Huang, R. Interfacial redox processes in memristive devices based on valence change and electrochemical metallization. *Faraday Discuss.* **2019**, *213* (0), 41−52.

(7) Zhao, X.; Zhang, X.; Shang, D.; Wu, Z.; Xiao, X.; Chen, R.; Tang, C.; Liu, J.; Li, W.; Lv, H.; Jiang, C.; Liu, Q.; Liu, M. Uniform, fast, and reliable LixSiOy-based resistive switching memory. *IEEE Electron Device Lett.* **2019**, *40* (4), 554−557.

(8) Yang, Y.; Huang, R. Probing memristive switching in nanoionic devices. *Nat. Electron.* **2018**, *1* (5), 274−287.

(9) Chen, J.-Y.; Huang, C.-W.; Chiu, C.-H.; Huang, Y.-T.; Wu, W.-W. Switching kinetic of VCM-based memristor: Evolution and positioning of nanofilament. *Adv. Mater.* **2015**, *27* (34), 5028−5033.

(10) Park, G.-S.; Kim, Y. B.; Park, S. Y.; Li, X. S.; Heo, S.; Lee, M.-J.; Chang, M.; Kwon, J. H.; Kim, M.; Chung, U. I.; Dittmann, R.; Waser, R.; Kim, K. In situ observation of filamentary conducting channels in an asymmetric Ta_2O_{5-x}/TaO_{2-x} bilayer structure. *Nat. Commun.* **2013**, *4* (1), No. 2382.

(11) Miao, F.; Strachan, J. P.; Yang, J. J.; Zhang, M.-X.; Goldfarb, I.; Torrezan, A. C.; Eschbach, P.; Kelley, R. D.; Medeiros-Ribeiro, G.; Williams, R. S. Anatomy of a nanoscale conduction channel reveals the mechanism of a high-performance memristor. *Adv. Mater.* **2011**, *23* (47), 5633−5640.

(12) Li, X.; Tung, C. H.; Pey, K. L. The nature of dielectric breakdown. *Appl. Phys. Lett.* **2008**, *93* (7), No. 072903.
(13) Li, C.; Gao, B.; Yao, Y.; Guan, X.; Shen, X.; Wang, Y.; Huang, P.; Liu, L.; Liu, X.; Li, J.; Gu, C.; Kang, J.; Yu, R. Direct observations of nanofilament evolution in switching processes in HfO_2-based resistive random access memory by in situ TEM studies. *Adv. Mater.* **2017**, *29* (10), No. 1602976.
(14) Cooper, D.; Baeumer, C.; Bernier, N.; Marchewka, A.; La Torre, C.; Dunin-Borkowski, R. E.; Menzel, S.; Waser, R.; Dittmann, R. Anomalous Resistance Hysteresis in Oxide ReRAM: Oxygen Evolution and Reincorporation Revealed by In Situ TEM. *Adv. Mater.* **2017**, *29* (23), No. 1700212.
(15) Baiutti, F.; Chiabrera, F.; Diercks, D.; Cavallaro, A.; Yedra, L.; López-Conesa, L.; Estradé, S.; Peiró, F.; Morata, A.; Aguadero, A.; Tarancón, A. Direct measurement of oxygen mass transport at the nanoscale. *Adv. Mater.* **2021**, *33* (48), No. 2105622.
(16) Hubbard, W. A.; Lodico, J. J.; Chan, H. L.; Mecklenburg, M.; Regan, B. C. Imaging dielectric breakdown in valence change memory. *Adv. Funct. Mater.* **2022**, *32* (2), No. 2102313.
(17) Barman, A.; Saini, C. P.; Sarkar, P. K.; Das, D.; Dhar, S.; Singh, M.; Sinha, A. K.; Kanjilal, D.; Gupta, M.; Phase, D. M.; Kanjilal, A. Nanoscale self-recovery of resistive switching in Ar^+ irradiated TiO^{2-x} films. *J. Phys. D: Appl. Phys.* **2017**, *50* (47), No. 475304.
(18) Lee, W.; Jung, H. J.; Lee, M. H.; Kim, Y.-B.; Park, J. S.; Sinclair, R.; Prinz, F. B. Oxygen surface exchange at grain boundaries of oxide ion conductors. *Adv. Funct. Mater.* **2012**, *22* (5), 965−971.
(19) Yang, Y.; Zhang, X.; Qin, L.; Zeng, Q.; Qiu, X.; Huang, R. Probing nanoscale oxygen ion motion in memristive systems. *Nat. Commun.* **2017**, *8* (1), No. 15173.
(20) Dagdeviren, O. E.; Mascaro, A.; Yuan, S.; Shirani, J.; Bevan, K. H.; Grütter, P. Ergodic and nonergodic dynamics of oxygen vacancy migration at the nanoscale in inorganic perovskites. *Nano Lett.* **2020**, *20* (10), 7530−7535.
(21) Belaidi, S.; Girard, P.; Leveque, G. Electrostatic forces acting on the tip in atomic force microscopy: Modelization and comparison with analytic expressions. *J. Appl. Phys.* **1997**, *81* (3), 1023−1030.
(22) Barth, C.; Foster, A. S.; Henry, C. R.; Shluger, A. L. Recent trends in surface characterization and chemistry with high-resolution scanning force methods. *Adv. Mater.* **2011**, *23* (4), 477−501.
(23) Sokolović, I.; Reticcioli, M.; Čalkovský, M.; Wagner, M.; Schmid, M.; Franchini, C.; Diebold, U.; Setvín, M. Resolving the adsorption of molecular O_2 on the rutile TiO_2(110) surface by noncontact atomic force microscopy. *Proc. Natl. Acad. Sci. U.S.A.* **2020**, *117* (26), 14827−14837.
(24) Heyde, M.; Simon, G. H.; Lichtenstein, L. Resolving oxide surfaces − From point and line defects to complex network structures. *Phys. Status Solidi (b)* **2013**, *250* (5), 895−921.
(25) Rodenbücher, C.; Bihlmayer, G.; Speier, W.; Kubacki, J.; Wojtyniak, M.; Rogala, M.; Wrana, D.; Krok, F.; Szot, K. Local surface conductivity of transition metal oxides mapped with true atomic resolution. *Nanoscale* **2018**, *10* (24), 11498−11505.
(26) Lanza, M.; Zhang, K.; Porti, M.; Nafría, M.; Shen, Z. Y.; Liu, L. F.; Kang, J. F.; Gilmer, D.; Bersuker, G. Grain boundaries as preferential sites for resistive switching in the HfO_2 resistive random access memory structures. *Appl. Phys. Lett.* **2012**, *100* (12), No. 123508.
(27) Ranjan, A.; Puglisi, F. M.; Molina-Reyes, J.; Pavan, P.; O'Shea, S. J.; Raghavan, N.; Pey, K. L. Spatially controlled generation and probing of random telegraph noise in metal nanocrystal embedded HfO_2 using defect nanospectroscopy. *ACS Appl. Electron. Mater.* **2022**, *4* (8), 3909−3921.
(28) Kumar, A.; Ciucci, F.; Morozovska, A. N.; Kalinin, S. V.; Jesse, S. Measuring oxygen reduction/evolution reactions on the nanoscale. *Nat. Chem.* **2011**, *3* (9), 707−713.
(29) Kurnia, F.; Cheung, J.; Cheng, X.; Sullaphen, J.; Kalinin, S. V.; Valanoor, N.; Vasudevan, R. K. Nanoscale probing of elastic−electronic response to vacancy motion in NiO nanocrystals. *ACS Nano* **2017**, *11* (8), 8387−8394.
(30) Rief, M.; Gautel, M.; Oesterhelt, F.; Fernandez, J. M.; Gaub, H. E. Reversible unfolding of individual Titin Immunoglobulin domains by AFM. *Science* **1997**, *276* (5315), 1109−1112.
(31) Bhushan, B.; Jung, Y. C. Wetting study of patterned surfaces for superhydrophobicity. *Ultramicroscopy* **2007**, *107* (10), 1033−1041.
(32) Mehonic, A.; Buckwell, M.; Montesi, L.; Munde, M. S.; Gao, D.; Hudziak, S.; Chater, R. J.; Fearn, S.; McPhail, D.; Bosman, M.; Shluger, A. L.; Kenyon, A. J. Nanoscale transformations in metastable, amorphous, silicon-rich silica. *Adv. Mater.* **2016**, *28* (34), 7486−7493.
(33) Mehonic, A.; Shluger, A. L.; Gao, D.; Valov, I.; Miranda, E.; Ielmini, D.; Bricalli, A.; Ambrosi, E.; Li, C.; Yang, J. J.; Xia, Q.; Kenyon, A. J. Silicon Oxide (SiO_x): A promising material for resistance switching? *Adv. Mater.* **2018**, *30* (43), No. 1801187.
(34) Ilyas, N.; Li, C.; Wang, J.; Jiang, X.; Fu, H.; Liu, F.; Gu, D.; Jiang, Y.; Li, W. A modified SiO_2-based memristor with reliable switching and multifunctional synaptic behaviors. *J. Phys. Chem. Lett.* **2022**, *13* (3), 884−893.
(35) Lombardo, S.; Stathis, J. H.; Linder, B. P.; Pey, K. L.; Palumbo, F.; Tung, C. H. Dielectric breakdown mechanisms in gate oxides. *J. Appl. Phys.* **2005**, *98* (12), No. 121301.
(36) Padovani, A.; Gao, D. Z.; Shluger, A. L.; Larcher, L. A microscopic mechanism of dielectric breakdown in SiO_2 films: An insight from multi-scale modeling. *J. Appl. Phys.* **2017**, *121* (15), No. 155101.
(37) Kimmel, A.; Sushko, P.; Shluger, A.; Bersuker, G. Positive and negative oxygen vacancies in amorphous silica. *ECS Trans.* **2009**, *19* (2), 3−17.
(38) Gao, D. Z.; El-Sayed, A.-M.; Shluger, A. L. A mechanism for Frenkel defect creation in amorphous SiO_2 facilitated by electron injection. *Nanotechnology* **2016**, *27* (50), No. 505207.
(39) Israelachvili, J. N. *Intermolecular and Surface Forces*; Academic Press: New York, 2011.
(40) Bhattacharjee, S.; Elimelech, M. Surface element integration: A novel technique for evaluation of DLVO interaction between a particle and a flat plate. *J. Colloid Interface Sci.* **1997**, *193* (2), 273−285.
(41) Shen, C.; Bradford, S. A.; Li, T.; Li, B.; Huang, Y. Can nanoscale surface charge heterogeneity really explain colloid detachment from primary minima upon reduction of solution ionic strength? *J. Nanopart. Res.* **2018**, *20* (6), No. 165.
(42) Snow, E. S.; Campbell, P. M. AFM fabrication of sub-10-nanometer metal-oxide devices with in situ control of electrical properties. *Science* **1995**, *270* (5242), 1639−1641.
(43) Stathis, J. H. Reliability limits for the gate insulator in CMOS technology. *IBM J. Res. Dev.* **2002**, *46* (2.3), 265−286.
(44) Buckwell, M.; Montesi, L.; Mehonic, A.; Reza, O.; Garnett, L.; Munde, M.; Hudziak, S.; Kenyon, A. J. Microscopic and spectroscopic analysis of the nature of conductivity changes during resistive switching in silicon-rich silicon oxide. *Phys. Status Solidi C* **2015**, *12* (1−2), 211−217.
(45) Yang, J. J.; Miao, F.; Pickett, M. D.; Ohlberg, D. A. A.; Stewart, D. R.; Lau, C. N.; Williams, R. S. The mechanism of electroforming of metal oxide memristive switches. *Nanotechnology* **2009**, *20* (21), No. 215201.
(46) Lo, C.-L.; Catalano, M.; Smithe, K. K. H.; Wang, L.; Zhang, S.; Pop, E.; Kim, M. J.; Chen, Z. Studies of two-dimensional h-BN and MoS_2 for potential diffusion barrier application in copper interconnect technology. *npj 2D Mater. Appl.* **2017**, *1* (1), No. 42.
(47) Ranjan, A.; Pey, K. L.; O'Shea, S. J. The interplay between drift and electrical measurement in conduction atomic force microscopy. *Rev. Sci. Instrum.* **2019**, *90* (7), No. 073701.
(48) Zhang, L.; Mitani, Y.; Satake, H. Visualization of progressive breakdown evolution in gate dielectric by conductive atomic force microscopy. *IEEE Trans. Device Mater. Reliab.* **2006**, *6* (2), 277−282.
(49) Fu, Q.; Wagner, T. Interaction of nanostructured metal overlayers with oxide surfaces. *Surf. Sci. Rep.* **2007**, *62* (11), 431−498.
(50) Cornil, D.; Rivolta, N.; Mercier, V.; Wiame, H.; Beljonne, D.; Cornil, J. Enhanced adhesion energy at Oxide/Ag interfaces for low-

https://doi.org/10.1021/acsaelm.3c00903
ACS Appl. Electron. Mater. 2023, 5, 5176−5186

emissivity glasses: Theoretical insight into doping and vacancy effects. *ACS Appl. Mater. Interfaces* **2020**, *12* (36), 40838−40849.
(51) Taylor, J. C. Platinum metallization on silicon and silicates. *J. Mater. Res.* **2021**, *36* (1), 211−234.
(52) Hu, X.; Cahill, D. G.; Averback, R. S. Dewetting and nanopattern formation of thin Pt films on SiO_2 induced by ion beam irradiation. *J. Appl. Phys.* **2001**, *89* (12), 7777−7783.
(53) Pretorius, R.; Harris, J. M.; Nicolet, M. A. Reaction of thin metal films with SiO_2 substrates. *Solid-State Electron.* **1978**, *21* (4), 667−675.
(54) Yang, Y.; Gao, P.; Li, L.; Pan, X.; Tappertzhofen, S.; Choi, S.; Waser, R.; Valov, I.; Lu, W. D. Electrochemical dynamics of nanoscale metallic inclusions in dielectrics. *Nat. Commun.* **2014**, *5* (1), No. 4232.
(55) Wang, Z.; Jiang, H.; Jang, M. H.; Lin, P.; Ribbe, A.; Xia, Q.; Yang, J. J. Electrochemical metallization switching with a platinum group metal in different oxides. *Nanoscale* **2016**, *8* (29), 14023−14030.
(56) Tea, E.; Huang, J.; Li, G.; Hin, C. Atomic bonding and electrical potential at metal/oxide interfaces, a first principle study. *J. Chem. Phys.* **2017**, *146* (12), No. 124706.
(57) Mortensen, K.; Klink, C.; Jensen, F.; Besenbacher, F.; Stensgaard, I. Adsorption position of oxygen on the Pt(111) surface. *Surf. Sci. Lett.* **1989**, *220* (2), L701−L708.
(58) Salmerón, M.; Brewer, L.; Somorjai, G. A. The structure and stability of surface platinum oxide and of oxides of other noble metals. *Surf. Sci.* **1981**, *112* (3), 207−228.
(59) Banerjee, R.; Liu, Q.; Tengco, J. M. M.; Regalbuto, J. R. Detection of ambient oxidation of ultrasmall supported Platinum nanoparticles with benchtop powder X-Ray diffraction. *Catal. Lett.* **2017**, *147* (7), 1754−1764.
(60) Solano, E.; Dendooven, J.; Ramachandran, R. K.; Van de Kerckhove, K.; Dobbelaere, T.; Hermida-Merino, D.; Detavernier, C. Key role of surface oxidation and reduction processes in the coarsening of Pt nanoparticles. *Nanoscale* **2017**, *9* (35), 13159−13170.
(61) McCabe, R. W.; Wong, C.; Woo, H. S. The passivating oxidation of Platinum. *J. Catal.* **1988**, *114* (2), 354−367.
(62) Ryl, J.; Burczyk, L.; Zielinski, A.; Ficek, M.; Franczak, A.; Bogdanowicz, R.; Darowicki, K. Heterogeneous oxidation of highly boron-doped diamond electrodes and its influence on the surface distribution of electrochemical activity. *Electrochim. Acta* **2019**, *297*, 1018−1027.
(63) Wang, M.; Simon, N.; Decorse-Pascanut, C.; Bouttemy, M.; Etcheberry, A.; Li, M.; Boukherroub, R.; Szunerits, S. Comparison of the chemical composition of boron-doped diamond surfaces upon different oxidation processes. *Electrochim. Acta* **2009**, *54* (24), 5818−5824.
(64) Shpilman, Z.; Gouzman, I.; Grossman, E.; Akhvlediani, R.; Hoffman, A. Oxidation of diamond films by atomic oxygen: High resolution electron energy loss spectroscopy studies. *J. Appl. Phys.* **2007**, *102* (11), No. 114914.
(65) Pehrsson, P. E.; Mercer, T. W.; Chaney, J. A. Thermal oxidation of the hydrogenated diamond (100) surface. *Surf. Sci.* **2002**, *497* (1), 13−28.
(66) Loh, K. P.; Xie, X. N.; Yang, S. W.; Zheng, J. C. Oxygen adsorption on (111)-oriented diamond: A study with ultraviolet photoelectron spectroscopy, temperature-programmed desorption, and periodic density functional theory. *J. Phys. Chem. B* **2002**, *106* (20), 5230−5240.
(67) Zhukovskii, Y. F.; Kotomin, E. A.; Jacobs, P. W. M.; Stoneham, A. M. Ab initio modeling of metal adhesion on oxide surfaces with defects. *Phys. Rev. Lett.* **2000**, *84* (6), 1256−1259.
(68) Stoneham, A. M.; Tasker, P. W. Image charges and their influence on the growth and the nature of thin oxide films. *Philos. Mag. B* **1987**, *55* (2), 237−252.
(69) He, J.-w.; Møller, P. J. On the defect center electron energy loss structures from MgO surfaces. *Chem. Phys. Lett.* **1986**, *129* (1), 13−16.
(70) Matsunaka, D.; Shibutani, Y. Effects of oxygen vacancy on adhesion of incoherent metal/oxide interface by first-principles calculations. *Surf. Sci.* **2010**, *604* (2), 196−200.
(71) Tosoni, S.; Pacchioni, G. Trends in adhesion energies of gold on MgO(100), rutile TiO_2(110), and CeO_2(111) surfaces: A comparative DFT study. *J. Phys. Chem. C* **2017**, *121* (51), 28328−28338.
(72) Burnham, N. A.; Colton, R. J.; Pollock, H. M. Interpretation of force curves in force microscopy. *Nanotechnology* **1993**, *4* (2), No. 64.
(73) Stathis, J. H. Percolation models for gate oxide breakdown. *J. Appl. Phys.* **1999**, *86* (10), 5757−5766.
(74) Larcher, L.; Padovani, A.; Vandelli, L. A simulation framework for modeling charge transport and degradation in high-k stacks. *J. Comput. Electron.* **2013**, *12* (4), 658−665.
(75) Butt, H.-J.; Cappella, B.; Kappl, M. Force measurements with the atomic force microscope: Technique, interpretation and applications. *Surf. Sci. Rep.* **2005**, *59* (1), 1−152.
(76) Cleveland, J. P.; Manne, S.; Bocek, D.; Hansma, P. K. A nondestructive method for determining the spring constant of cantilevers for scanning force microscopy. *Rev. Sci. Instrum.* **1993**, *64* (2), 403−405.
(77) Edwards, S. A.; Ducker, W. A.; Sader, J. E. Influence of atomic force microscope cantilever tilt and induced torque on force measurements. *J. Appl. Phys.* **2008**, *103* (6), No. 064513.

https://doi.org/10.1021/acsaelm.3c00903
ACS Appl. Electron. Mater. 2023, 5, 5176−5186